Research Article | Vol. 27, No. 2 | 21 Jan 2019 | OPTICS EXPRESS 1401
Optics EXPRESS

Tuning forks with optimized geometries for quartz-enhanced photoacoustic spectroscopy

PIETRO PATIMISCO,[1] ANGELO SAMPAOLO,[1] MARILENA GIGLIO,[1] STEFANO DELLO RUSSO,[1] VERENA MACKOWIAK,[2] HUBERT ROSSMADL,[2] ALEX CABLE,[3] FRANK K. TITTEL[4] AND VINCENZO SPAGNOLO[1*]

[1]*PolySense Lab - Dipartimento Interateneo di Fisica, University and Politecnico of Bari, Via Amendola 173, Bari, Italy*
[2]*Thorlabs GmbH, Hans-Boeckler-Straße 6, 85221 Dachau, Germany*
[3]*Thorlabs, Inc., 56 Sparta Ave., Newton, NJ 07860, USA*
[4]*Department of Electrical and Computer Engineering, Rice University, 6100 Main Street, Houston, TX 77005, USA*
[*]*vincenzoluigi.spagnolo@poliba.it*

Abstract: We report on the design, realization, and performance of novel quartz tuning forks (QTFs) optimized for quartz-enhanced photoacoustic spectroscopy (QEPAS). Starting from a QTF geometry designed to provide a fundamental flexural in-plane vibrational mode resonance frequency of ~16 kHz, with a quality factor of 15,000 at atmospheric pressure, two novel geometries have been realized: a QTF with T-shaped prongs and a QTF with prongs having rectangular grooves carved on both surface sides. The QTF with grooves showed the lowest electrical resistance, while the T-shaped prongs QTF provided the best photoacoustic response in terms of signal-to-noise ratio (SNR). When acoustically coupled with a pair of micro-resonator tubes, the T-shaped QTF provides a SNR enhancement of a factor of 60 with respect to the bare QTF, which represents a record value for mid-infrared QEPAS sensing.

1. Introduction

Optical techniques operating in the mid-infrared spectral regions are capable of excellent trace gas sensing performances, together with high sensitivity and selectivity [1,2] due to the presence of strong ro-vibrational absorption bands of many molecules. Photoacoustic spectroscopy (PAS) is a sensing technique that does not require the use of an optical detector and troublesome optical alignments, but nevertheless is capable of performing trace gas measurements at sub-parts-per-trillion concentration levels [3,4]. PAS is based on the detection of sound waves generated by gas absorption of modulated optical radiation. Quartz tuning forks (QTFs) have shown a great potential as sound transducers, leading to a well-established variant of PAS, named quartz-enhanced photoacoustic spectroscopy (QEPAS) [5]. The confinement of the acoustic energy between the prongs of the QTF, combined with high quality factors, enabled the detection of weak photoacoustic excitation within very small gas volumes. Since its introduction in 2002, standard low-cost QTFs with resonance frequencies at 32.7 kHz are typically employed in QEPAS sensors [6]. The QTF is typically coupled with a pair of tubes, acting as an organ pipe resonator to probe the sound wave [7,8]. The acoustic detection module composed of the QTF and micro-resonator tubes constitutes the QEPAS spectrophone, which is the core of any QEPAS sensor. In QEPAS sensing, the light source is focused between QTF prongs and sound waves produced by the modulated absorption of the gas are generated between the QTF prongs, forcing them to oscillate back and forth (in-plane anti-symmetrical modes). The main problem in the realization of a standard QEPAS sensor is the focalization of the laser beam within the 300 μm-gap between the standard QTF prongs without touching both micro-resonator tubes and the QTF. This is crucial in order to avoid the generation of a photo-thermal noise contribution which would be added to the piezoelectric

#340626 https://doi.org/10.1364/OE.27.001401
Journal © 2019 Received 25 Jul 2018; revised 31 Oct 2018; accepted 4 Nov 2018; published 16 Jan 2019

Optics EXPRESS

signal [9]. When laser modulation occurs at one of resonance frequencies of in-plane piezoelectrically active modes, the induced strain field generates surface electric charges proportional to the intensity of the sound waves incident on the QTF prongs. When the light is periodically absorbed by the gas, the energy excess is mainly dissipated through non-radiative relaxation processes, involving vibrational and rotational excited states. Sound waves are then generated via energy transfer from excited states to translational degrees of freedom. The ability of the gas target to periodically relax the excess of energy depends on the modulation frequency (i.e. the resonance frequency of the QTF in-plane mode) of the incident laser radiation and differs for each gas [10,11]. With respect to the standard PAS, QEPAS operates at higher resonance frequencies. For slow relaxing gases, such as CO, CO_2 and NO a QEPAS sensor operational frequency as high as 32.7 kHz, like in standard QTFs, can limit the sound wave generation efficiency [12]. These considerations suggested directions for the realization of improved QTFs: i) reduction of the QTF fundamental frequency, ii) increase the prongs spacing in order to facilitate the optical alignments and minimize the photo-thermal noise level. Starting in 2013, custom QTFs have been realized in QEPAS sensors following these two guidelines [13]. Larger prongs spacing led to the use of the QEPAS technique with laser sources having a poor spatial beam quality as well as operating in the terahertz spectral range [13,14]. The implementation of a single-tube as acoustic micro-resonator system is another achievement [15]. Lowering the fundamental frequency also opened the way to the use of first overtone mode in QEPAS sensing [16,17], leading to a double-antinode QEPAS configuration [18] and simultaneous dual-gas detection by exciting with two laser sources both the fundamental and first overtone QTF flexural modes, simultaneously [19]. However, guidelines for QTFs optimized for QEPAS operation are still not well defined.

This paper reports an investigation of the influence of prong sizes on both the resonance frequency and on the quality factor of the fundamental flexural mode, leading to the design of a quartz tuning fork optimized for QEPAS sensing. Starting from this design, two novel geometries were proposed: one with T-shaped prongs to optimize the strain field between the prongs and their support and the other one having prongs with grooves carved on the central sides in order to reduce the QTF electrical resistance. After determining the resonance properties, the investigated QTF samples were implemented in a QEPAS setup to test their photoacoustic response. The QTF providing the best performance in terms of signal-to-noise ratio (SNR) was acoustically coupled with a dual-tube micro-resonator system. The influence of the geometrical parameters on the photoacoustic response, namely the internal diameter and the length of the two tubes together with the spacing between the tube and the QTF, was also investigated to determine the optimal micro-resonator geometry.

2. Guidelines for the design of quartz tuning forks

The photoacoustic signal is proportional to the product $Q \cdot P \cdot \alpha$, where Q is the QTF resonance quality factor, α is the gas target absorption coefficient and P is the laser power [17]. The straightforward approach to design QTFs optimized for QEPAS sensing is to reduce the resonance frequency while keeping high the quality factor. The dependence of the resonance frequency and related quality factor on the QTF relevant dimensions has been investigated in [20], where a set of QTFs with different values of spacing between the prongs and their sizes was analyzed. This study showed that resonance frequencies of in-plane flexural modes can be well predicted by using the Euler-Bernoulli equation. Considerations about the quality factor are more challenging. The Q-factor depends on all the energy dissipation mechanisms occurring in a vibrating prong of a QTF. The main contributions are due to damping by the surrounding fluid, the interaction of the prong with its support and thermo-elastic damping [21]. All these loss mechanisms strongly depend on the QTF prongs size. Although several theoretical models have been proposed to describe the dependence of each loss mechanism on the prongs geometry [22–24], there is no theoretical model capable to take into account all the

Optics EXPRESS

dissipation mechanisms in one, consistent formulation. An experimental investigation described in [21] on the QTF fundamental flexural mode resonance at atmospheric pressure demonstrates that the overall quality factor can be phenomenologically related to the prong sizes by:

$$Q = 3.78 \cdot 10^5 \frac{wT}{L} \quad (1)$$

where w, T and L are the crystal thickness, the prongs width and the prongs length, respectively, all expressed in mm-units. This relation suggests that the overall quality factor of the fundamental mode can be increased by reducing the prong length and increasing both thickness and crystal width. Conversely, according to Euler-Bernoulli model, the resonance frequency of the fundamental flexural mode increases as the ratio between the prong thickness and its squared length [20]. When the crystal thickness is fixed, the quality factor scales linearly as the ratio T/L and Eq. (1) becomes $Q = 9.45 \cdot 10^4\ T/L$, for $w = 0.25$ mm, at atmospheric pressure. A MATLAB-based software was realized to relate the quality factor and the resonance frequency at different prong geometries. For each fixed prong geometry (T, L), the software calculates the resonance frequency and the related Q-factor, and plots ordered points on the x- (frequencies, f) and y- (Q-factors) axis of the coordinate plane. By ranging L from 3 mm to 20 mm and T from 0.2 mm to 3.0 mm, while keeping w at a fixed value of 0.25 mm, the calculated ordered points (Q, f) are shown in Fig. 1.

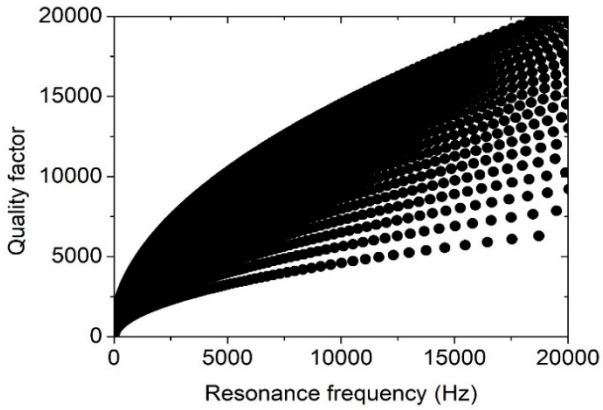

Fig. 1. Q-factor values plotted as a function of the resonance frequency for different prong lengths and thicknesses of quartz tuning fork of crystal width $w = 0.25$ mm, at atmospheric pressure.

The graph clearly shows that for a selected resonance frequency, different prong sizes can be chosen, providing quality factors values spanning in a certain range. Moving to low resonance frequencies, this range of possible quality factor values, as well as the Q-factor values itself, is reduced. In particular, QTFs with a resonance frequency lower than 10 kHz cannot ensure a Q-factor higher than 15,000, at atmospheric pressure. For a novel generation of QTFs optimized for QEPAS operation, a resonance frequency of ~16 kHz (a half of the standard 32.7 kHz) was selected. At $f = 16$ kHz, L and T values (with $w = 0.25$ mm) maximizing the quality factor (18,000) are 9.4 mm and 2.0 mm, respectively. In a first step, starting with this prong geometry we designed two QTFs differing only in the prong spacing: QTF-S08 having a prong spacing of 0.8 mm, and QTF-S15 with a prong spacing of 1.5 mm. With all other geometrical parameters being identical, a comparison between them in terms of QEPAS performance will allow establishing the influence of the prong spacing on the QTF frequency and Q-factor, as well as on the amount of radiation incident on the prong surface, which typical affects the QEPAS sensor noise level.

Optics EXPRESS

2.1 T-shaped tuning forks

When prongs of a tuning fork are vibrating at a resonance mode frequency, the stress produced along the prong induces a local polarization of quartz and charges appearing on its surface. This charge can be collected by electrical contacts appropriately deposited along the QTF prongs. The polarization depends on the stress field by the quartz piezoelectric tensor. An increase of the amplitude of the stress field produces an increase of the piezoelectrically induced charges, and subsequently an enhancement of the QTF current signal [25]. There are no analytical models to predict the intensity distribution of the stress field along QTF prongs when the prong deformation is caused by the fundamental flexural mode. For this reason, commercial finite element software COMSOL Multiphysics was used to simulate the QTF geometry and to estimate the stress field distribution along prong. With QTF prong sizes derived in previous section, i.e. L = 9.4 mm and T = 2.0 mm (and w = 0.25 mm), the obtained stress field distribution is shown in Fig. 2(a).

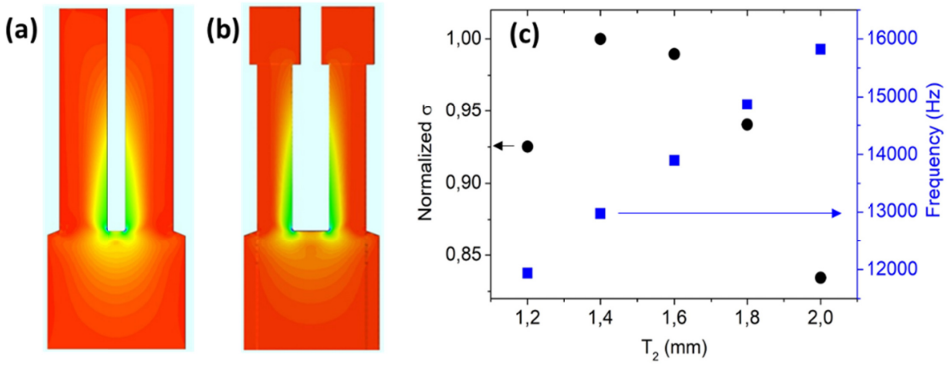

Fig. 2. Stress field distribution for QTF-S08 (a) and QTF-S08-T (b) simulated by using COMSOL MultiPhysics. (c) Normalized stress field intensity σ (●) and resonance frequency (■) as a function of T_2 for QTF-S08-T.

The stress field is mainly localized at the junction between the prong base and the QTF support and extends in the support area. When a QTF is used in a QEPAS sensor, the laser beam is focused between the QTF prongs, not far from the prong top, and it can be treated as the acoustic source for the prong deformation. In other words, a prong deformation results from a stress field induced by pressure waves hitting close to the prongs top. If some extra mass is added to the free end of the prong, a change of the stress field distribution is expected. Starting from these considerations, a modified geometry for QTF prongs is proposed, in which the prong thickness T is not constant along the prong axis. The thickness function $T(x)$ of the prong is thought out to be a piecewise function that can be written as:

$$T(x) = \begin{cases} T_1 & x \in [0, L_0] \\ T_2 & x \in [L_0, L_1] \end{cases} \quad (2)$$

This prong geometry will be referred as a T-shaped prong. Starting from the prong geometry defined in the previous section (T_1 = 2 mm, L = 9.4 mm and w = 0.25 mm), L_0 was determined by considering the effective mass (which is an estimation of the effective vibrating mass for a prong at the fundamental mode), resulting in about 1/4 of the mass of one of the prongs [26], i.e. $L_0 = L/4$ = 2.4 mm. T_2 was determined by using COMSOL Multiphysics, spanning T_2 from 2.0 mm to 1.2 mm as a function of the stress field intensity. The obtained results are reported in Fig. 2(c). We found that T_2 = 1.4 mm is the prong thickness value maximizing the stress field intensity. The related stress field distribution is shown in Fig. 2(b). The simulation shows that the T-shape results in a better distribution of

Optics EXPRESS

the stress field associated with the vibration along the internal prong surface, where the generated charges are collected, when performing QEPAS experiments. A decrease of the resonance frequency of the fundamental mode is also predicted, as depicted on the right y-axis in Fig. 2(c). The realized modified QTF geometry with T-shaped prong has dimensions of T_1 = 2.0 mm, T_2 = 1.4 mm, L_0 = 2.4 mm and L_1 = 9.4 and will be named hereafter as QTF-S08-T.

2.2 Grooves tuning forks

As deduced from Fig. 1, when the resonance frequency is reduced, the quality factor is also negatively affected. A reduction of the quality factor involves an increase of the electrical resistance [20,27]. To keep the electrical resistance low, the coupling between the electrodes and the resonance mode must be optimized. This can be achieved by carving rectangular grooves on both surfaces of each prong of QTF-S08. Depositing the central electrodes on the carved surfaces provides an increase of the piezoelectric coupling and at the same time a decrease of the equivalent electrical resistance, representing the loss parameter in the equivalent conventional resonator circuit. All these modifications do not affect the resonator quality factor. The QTF-S08 with grooves applied on both prongs is schematically shown in Fig. 3(a)-(c) and will be named hereafter as QTF-S08-G.

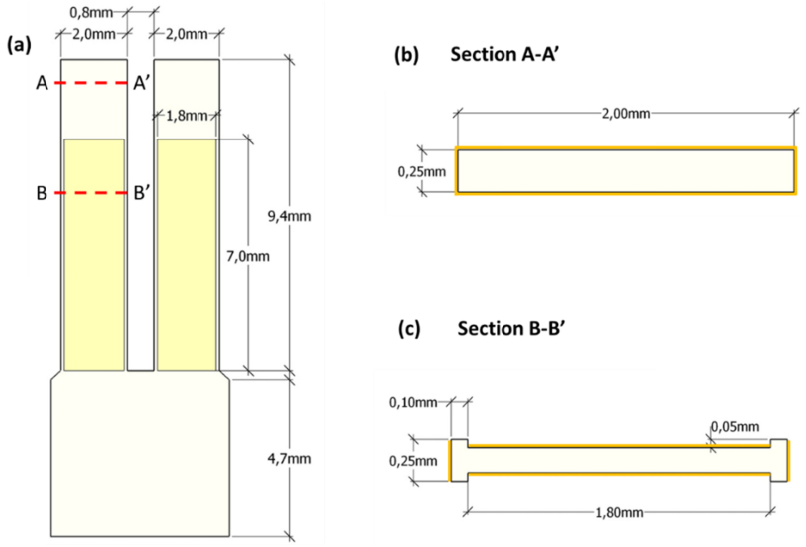

Fig. 3. (a) Front view with sizes of the QTF-S08-G. Dark yellow areas represents grooves applied on both sides of QTF prongs. (b) Cross-section of QTF-S08-G prongs along AA'. (c) Cross-section of the QTF-S08-G prongs along BB'.

These grooves were realized by carving 50 µm of the upper and lower crystal surfaces and the width of the areas placed between the grooves and the lateral edges of the prong was fixed to 100 µm, so that the resonator maintains a good mechanical resistance and sufficient stiffness. The carved area corresponds to 40% of the total crystal thickness.

3. Resonance properties

The QTFs response can be obtained by exciting the resonators electrically. The new generation of QTFs (QTF-S08, QTF-S08-T, QTF-S08-G and QTF-S15) reported in this work will be compared with QTFs reported in [20] showing the best performance, namely QTF#1 vibrating at the first overtone mode and QTF#2 at the fundamental mode. The experimental setup used to characterize QTFs via electrical excitation is schematically depicted in Fig. 4(a).

Optics EXPRESS

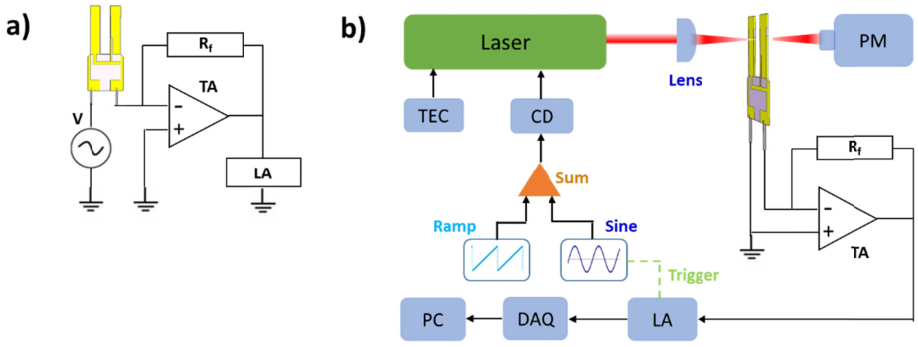

Fig. 4. (a) Circuit diagram for QTF electrical excitation. A sinusoidal voltage is applied to the QTF. The QTF current output is converted to a voltage signal by means of a transimpedance amplifier (TA) with a feedback resistor of R_F = 10 MΩ. The signal is then demodulated by a lock-in amplifier (LA). (b) Schematic of the QEPAS trace gas sensor system using a quantum cascade laser as the excitation source. The laser beam is focused between QTF prongs by means of a lens. TEC: Temperature controller. CD: current driver. PC: personal computer. DAQ: Data Acquisition Card. PM: Power Meter.

The QTF is electrically excited by a sinusoidal voltage signal, resulting in a piezoelectric charge displacement on its prongs via inverse piezoelectric effect. The QTF current is converted to a voltage signal by means of the trans-impedance amplifier (TA). The lock-in amplifier (LA) demodulates the voltage signal at the same frequency of the waveform generator signal. To determine the resonance properties of QTFs, namely the resonance frequency, the related quality factor and the electrical resistance, the frequency of the function generator was varied step-by-step. It is well-known that the resonance curves of QTFs vibrational flexural modes have a Lorentzian line-shape. The resonance peak broadening is proportional to the energy losses occurring in the vibrating prongs. Furthermore, the larger the broadening, the higher are the losses. The quality factor Q can be calculated as the ratio between the resonance frequency and the full-width-half-maximum (FWHM) value of the resonance curve. Starting from the theoretical resonance frequency values predicted by the Euler-Bernoulli model, the response of all QTFs was investigated in a spectral range around the theoretical value of the fundamental flexural in-plane mode. The spectral responses of the new generation of QTFs, at atmospheric pressure in air, are shown in Fig. 5(a)-(d).

Optics EXPRESS

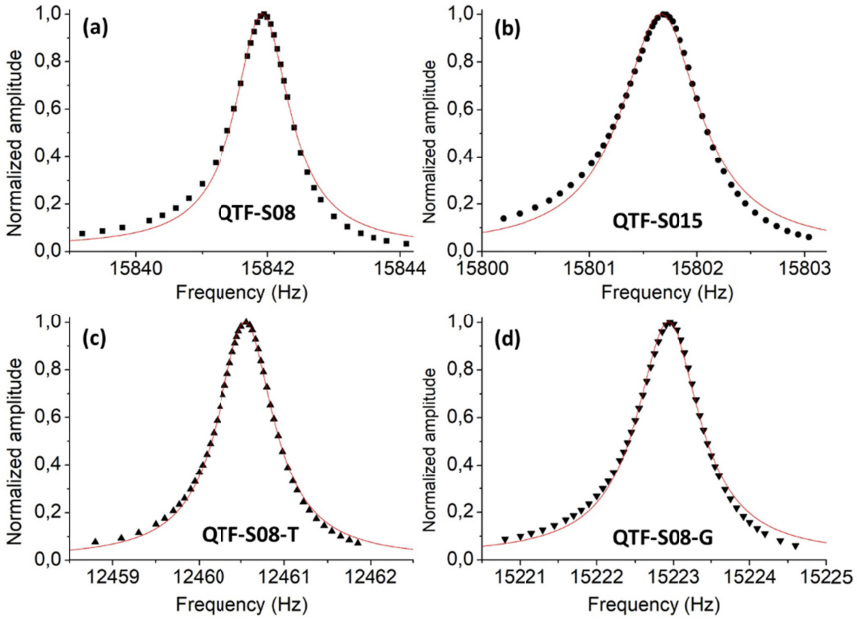

Fig. 5. Resonance curves of (a) QTF-S08 (■), (b) QTF-S015 (●), (c) QTF-S08-T (▲) and (c) QTF-S08-G (▼) measured at a fixed excitation level V_0 = 0.5 mV at atmospheric pressure in standard air near the fundamental oscillation mode. The red solid lines indicate the best Lorentzian fit.

The small left-right asymmetry for in-phase components with respect to the curve peak are due to parasitic currents caused by stray capacitance between the two pins of the QTF, which dominated away from the resonance frequency [28]. In Table 1, resonance frequencies, *Q*-factors and electrical resistance values of the investigated QTFs are compared with results obtained with the first overtone mode of QTF#1 at 17787.95 Hz and fundamental mode of QTF#2 falling at 7220.45 Hz, together also with standard 32.7 kHz-QTF [20]. Assuming that the crystal width *w* is not affected by the QTFs fabrication process, *L* and *T* uncertainties are estimated to be ~25 μm. By using the law of propagation of uncertainty for both Euler-Bernoulli equation and Eq. (1), we estimated an uncertainty of both the resonance and the Q-factor predicted values of ~1%.

Table 1. Resonance frequencies (f_0), quality factors (Q) and electrical resistance (R) of QTF-S08, QTF-S08-G, QTF-S08-T, QTF-S15, QTF#1, QTF#2 and standard 32.7 kHz-QTF.

QTF	f_0 (Hz)	Q	R (kΩ)
QTF-S08	15841.92	15710	162.8
QTF-S15	15801.66	15400	141.7
QTF-S08-T	12460.55	15540	157.5
QTF-S08-G	15222.93	15050	104.3
QTF#1	17787.95	14890	183.0
QTF#2	7220.45	8910	301.7
32 kHz-QTF	32760.83	13690	94.6

QTF-S08 and QTF-S15 share the same geometrical characteristics for each prong and differ only in the spacing between the prongs. The small difference (~ 2.5 μm) in the measured resonance frequencies implies that the prong spacing does not affect the resonance properties of the QTF and thereby the two prongs can be considered almost uncoupled. QTF-S08 and QTF-S15 also share almost the same *Q*-factor value (15,710 and 15,400, respectively), about 13% different from the predicted value of ~ 18,000. This means that the combination between

Optics EXPRESS

the Euler-Bernoulli model and the empirical dependence of the quality factor with prong width/length ratio is an efficient tool for the prediction of the quality factor values. Even if the resonance frequency of both QTF-S08 and QTF-S15 is almost a half of the standard 32.7 kHz-QTF, higher quality factors were measured. QTF-S08-G showed a resonance frequency about 4% lower than QTF-S08. Although the Euler-Bernoulli model does not predict a dependence of the resonance frequency on the crystal thickness w, 50 μm-grooves carving on both surface slightly affects the rectangular geometry of the prong and produces a small shift of the resonance frequency. For QTF-S08-T, a lower resonance frequency was measured with respect to QTF-S08 and QTF-S15, as predicted by COMSOL simulations, due to the non-uniformity of the moments of inertia along the prong section. For QTF-S08-T, a quality factor of 15,260 was measured. Although the prong T-geometry leads to a decrease of the prong width from 2 mm to 1.4 mm starting from 2.4 mm far from prong top, the quality factor was not affected. A comparison of the QTF#2 with the new generation QTFs shows that the latter exhibits higher quality factors and higher resonance frequencies, in agreement with the calculation shown in Fig. 1. A more interesting comparison can be performed when considering QTF#1 operating at the first overtone mode. QTF#1 has the fundamental flexural mode at 2.87 kHz with a quality factor of ~ 5,000 and the first overtone mode at 17.8 kHz with a quality factor as high as ~ 14,890. Therefore, by moving from the fundamental to the overtone mode leads to an increase of the resonance quality factor. This behavior can be explained by considering that air damping is strongly reduced when the resonance frequency increases [29] and support losses start to dominate when overtone modes are excited [30]. The new generation QTFs reached the same Q-factor values range of QTF#1 when they vibrate at the fundamental mode and this is useful in terms of QEPAS performance. T-shaping the prongs does not affect the electrical resistance, being nearly identical the electrical resistance measured for QTF-S08 and QTF-S08-T. While, a comparison of QTF-S08 and QTF-S08-G, clearly demonstrates that adding grooves on the prongs surfaces reduces the electrical resistance from 162.9 kΩ (QTF-S08) to 104.3 kΩ (QTF-S08-G), while Q-factor and resonance frequency are only slightly affected and thereby providing an improvement in terms of the QEPAS performance.

4. Photoacoustic response

To verify all assumptions, we employed all QTFs in the QEPAS setup, depicted in Fig. 4(b). A single-mode continuous-wave quantum cascade laser (QCL) was used as the excitation source to generate photoacoustic signals. The QCL targeted a water vapor absorption line falling at 1297.19 cm^{-1}, having intensity of $3.6 \cdot 10^{-22}$ cm/molecule [31]. The laser beam was focused between the QTF prongs using a ZnSe lens with a focal length of 50 mm. An aluminum enclosure equipped with two mid-IR AR-coated windows was realized in order to accommodate and easily switch the QTFs. The housing was filled by standard air with a fixed 1.7% water vapor concentration at atmospheric pressure. The QEPAS sensor operated with a wavelength modulation and dual-frequency detection approach, i.e. the laser beam is wavelength-modulated at a half of the selected resonance frequency while the lock-in amplifier demodulates the QTF signal at the resonance frequency. The absorption line is acquired by applying a slow ramp to the current driver allowing a linear wavelength-scan. As a first step, the vertical position of the laser beam focus along the QTF axis (as shown in Fig. 6(a)) has to be optimized in terms of the QEPAS signal. To study the dependence of the QEPAS signal intensity (proportional to the total momentum generated by the pressure wave) as a function of the vertical position of the laser beam, the laser beam focus was moved from the top to the bottom along the QTF axis between the two prongs.

Optics EXPRESS

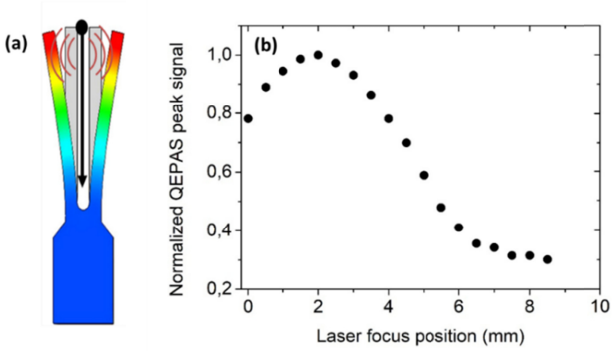

Fig. 6. (a) Sketch of a QTF depicting the prong deflection at the fundamental mode while an acoustic source is located between the prongs. The arrow indicates the QTF axis. (b) Normalized QEPAS peak signal acquired at different laser focus position measured from the top of the QTF axis.

The experimental QEPAS peak signals, normalized to the highest value, obtained for QTF-S08-T at different laser focused spot positions are shown in Fig. 6(a). The laser focus position maximizing the QEPAS signal is 2 mm far from the QTF top, between the two prongs. The same result was obtained for QTF-S08, QTF-S08-G and QTF-S15. For the fundamental mode, the optimum laser beam position is shifted towards the prong base with respect to the antinode vibrational point, theoretically located on the top of the prong. This can be explained by considering that the closer to the prong top is the vertical position of the spherical-like acoustic source, the larger is the fraction of the pressure wave not hitting a prong [17]. In all new generation QTFs, the laser beam was focused between the prongs, 2 mm far from the top. The QEPAS spectral scans of the selected water vapor absorption line obtained for the new generation QTFs, all operating at the fundamental mode, are shown in Fig. 7(a)-(d).

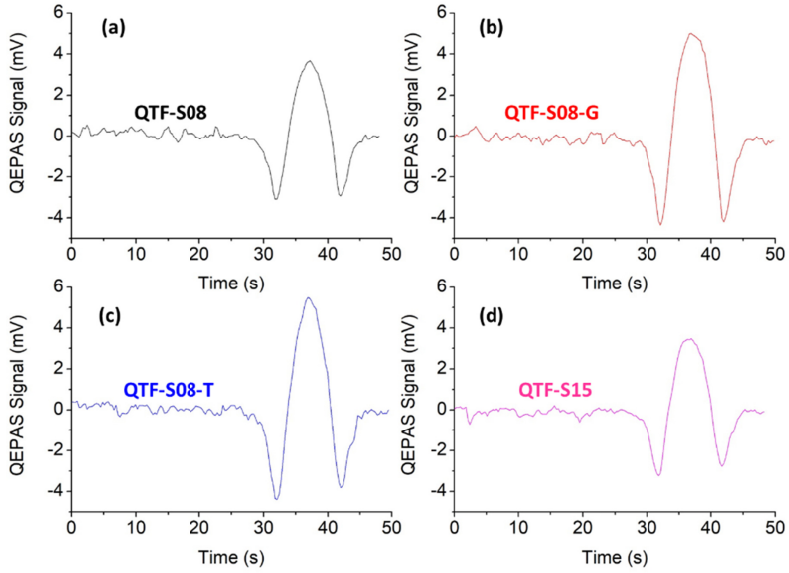

Fig. 7. QEPAS spectral scans of 1.7% water concentration in air for the fundamental flexural mode of QTF-S08 (a), QTF-S08-G (b), QTF-S08-T (c) and QTF-S15 (d). All scans were recorded with a 100 ms lock-in integration time.

Optics EXPRESS

The largest QEPAS signal was measured with the QTF-S08-T (5.48 mV), about 1.5 times higher than that measured with QTF-S08. The T-shaped prong designed starting from a rectangular prong provided two advantages: i) a reduction of the resonance frequency with no influence on the quality factor; ii) an increase of the stress field along the prongs lateral surface, leading to an increase of collected piezoelectric charges. Both advantages are beneficial for QEPAS sensor performance. QTF-S08 provides a QEPAS signal ~ 6% higher than QTF-S15. This means that even if the electro-elastic properties of QTFs are not influenced by the prong spacing, this parameter can influence the acousto-electric transduction efficiency, i.e., the conversion efficiency of the amplitude of the acoustic wave in piezoelectric charge production. The larger is the prong spacing the lower is the sound wave intensity hitting the internal surface of the prong. QTF-S08-G showed a QEPAS signal 1.36 times higher than QTF-S08, demonstrating that even if the grooves on the prong surface slightly affect the resonance frequency and the *Q*-factor, a decrease of the electrical resistance is more beneficial in terms QEPAS performance. QTF#1, QTF#2 and a standard 32.7 kHz-QTF were also tested with the same experimental conditions. The laser beam was focused 9.5 mm, 1.2 mm and 0.6 mm far from the top for QTF#1, QTF#2 and standard 32.7 kHz-QTF, respectively [17]. All new generation QTFs resulted in a better QEPAS performance with respect QTF#1 and QTF#2 in terms of peak signal. In particular, a comparison shows that the best QTF of the new QTF generation (QTF-S08-T) exhibits a QEPAS signal 4.2 times higher than QTF#1. In the graphs shown in Fig. 7(a)-(d), the range between 0 s and 24 s is free from absorption features. Hence, this range was used for the estimation of the 1σ noise level for all four QTFs. The 1σ noise level measured for all bare new generation QTFs was ~0.26 mV, for both prong spacings of 0.8 mm (QTF-S08, QTF-S08-T, QTF-S08-G) and 1.5 mm (QTF-S15), demonstrating that a prong spacing of 0.8 mm is large enough to ensure that a negligible portion of light hits the internal surface of prongs.

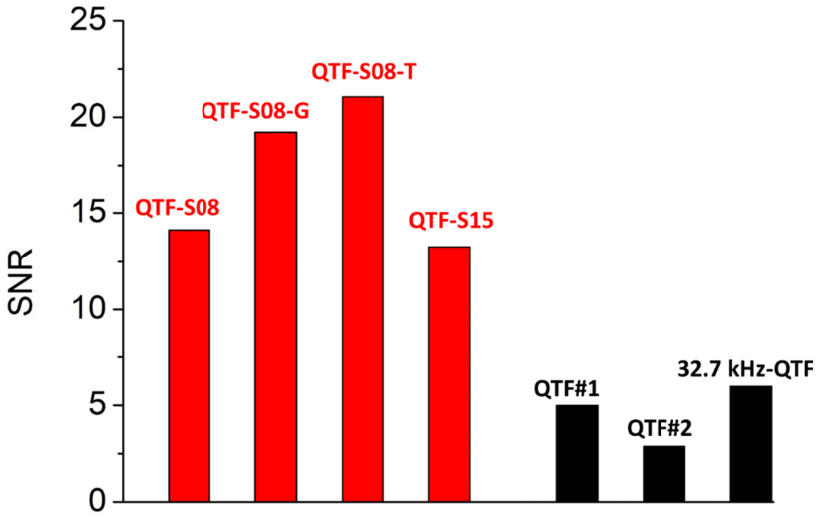

Fig. 8. SNR of QTF-S08, QTF-S08-G, QTF-S08-T and QTF-S15 compared with those acquired for QTF#1, QTF#2 and standard 32.7 KHz-QTF (black bars).

However, the most important parameter to compare different QEPAS sensors is the signal-to-noise ratio (SNR) defined as the ratio between the QEPAS peak signal and 1σ fluctuations of the signal in a spectral range (i.e. laser current range) where no optical absorptions are detected. In Fig. 8, a comparison between the investigated QTFs, together with QTF#1, QTF#2 and a standard 32.7 kHz-QTF, is shown in terms of the QEPAS SNR. All new generation QTFs showed the highest SNR values with respect to QTF#1 and QTF#2

Optics EXPRESS

and the standard 32.7 kHz-QTF, the latter showing also the highest noise level (9.4 times higher than the new generation QTFs) due to its small prong spacing of 0.3 mm.

5. T-shaped tuning fork with dual-tube micro-resonator

As demonstrated in Section 4, QTF-S08-T provides the highest QEPAS SNR. Hence, it is an excellent candidate for the realization of a spectrophone for QEPAS sensors. A spectrophone is typically composed by a QTF acoustically coupled with a pair of micro-resonator tubes, acting as amplifiers for the sound wave. The QTF is typically positioned between the tubes to probe the acoustic vibration excited in the absorbing gas contained inside the tubes [5–8]. A V-groove with a cylindrical hole was used to locate the two tubes at a fixed distance from the QTF. The geometrical parameters influencing the sensor performance are: the internal diameter and the length of the two tubes, together with the spacing between the tube and the surface of the QTF. In [8], a detailed investigation of geometrical parameters of the microresonator tubes as well as their influence on QEPAS sensing performance is reported. The first parameter to be optimized is the distance between the tubes and the internal surface of the prong. The gaps size between the QTF and the tubes is a difficult parameter to be controlled during the spectrophone assembly and it has a significant effect on its final performance. Two tubes having a length of 13.3 mm and internal diameter of 1.52 mm were placed at different distances from the prongs, spanning from 70 μm to 2.0 mm. The QEPAS peak signal measured as a function of the tube-QTF distance is plotted in Fig. 9.

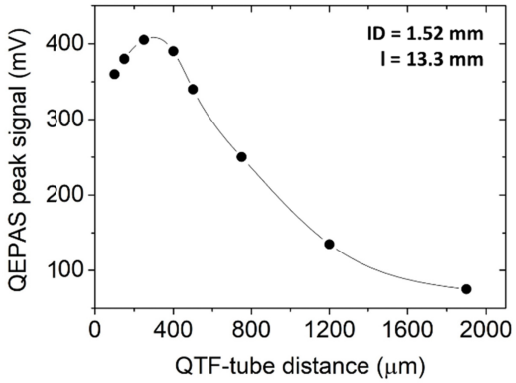

Fig. 9. QEPAS peak signal as a function of the distance between the tube and the QTF. Solid lines serve as convenient visual guides.

The distance between QTF and tubes maximizing the SNR is 200 μm. However, in the range 150 μm - 300 μm, the curve in Fig. 9 shows a quasi-plateau. Indeed, when changing the tube-QTF distance from 100 μm to 380 μm the QEPAS signal varies by less than 7%. The QEPAS signal approaches asymptotically that achieved with the bare QTF when the distance between the tubes and the QTF becomes larger than 2000 μm and rapidly increases when this distance is reduced, confirming that the shorter the QTF-tube distance the higher is the acoustical coupling between them. When the distance is shorter than 120 μm, the SNR decreases because of damping effects generated by the short distance between the tube and the QTF. The length of two tubes is correlated with the sound wavelength at the QTF resonance frequency (λ = 27.6 mm) [7,8]. Assuming that the left and right tubes are considered as a single tube neglecting the gap, each tube should be cut to a $\lambda/4$ length (l = 6.9 mm) to form a half-wave resonator. Instead, if the gap between the tubes is large enough to make them almost independent, each tube length should be $\lambda/2$ (l = 13.8 mm). Hence, we tested tubes having lengths between $\lambda/4$ and $\lambda/2$, i.e., 10 mm, 11 mm, 12.4 mm, 13 mm, 14 mm and 15 mm. The choice of the optimal ID is related to the QTF prongs spacing. When the tube diameter is larger than the prongs spacing, the gap between two tubes becomes less

Optics EXPRESS

important and the tubes are well acoustically coupled with the QTF. When the tube diameter becomes comparable with the prongs spacing, the acoustic coupling between tubes and QTF decreases. In addition, for small tube diameters a photothermal noise contribution to the QEPAS signal can arise, due to portion of the laser beam touching parts of the spectrophone. For this reason, tubes with IDs < 1 mm have not been taken into account. Hence, six different tubes with internal diameters ID = 1.36 mm, 1.41 mm, 1.52 mm, 1.59 mm, 1.83 mm and 2.06 mm have been investigated. As representatives, in Fig. 10, the QEPAS peak values are plotted as a function of the tube lengths, for ID = 1.41 mm, 1.59 mm and 2.06 mm.

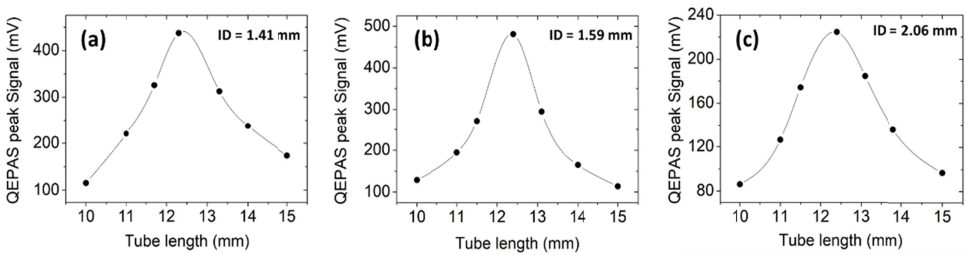

Fig. 10. QEPAS peak signals measured with three different spectrophones employing acoustic resonator tubes with an ID = 1.41 mm (a), 1.59 mm (b) and 2.06 mm (c) as a function of the tube length. Solid lines serve as convenient visual guides.

For all internal diameters investigated, the QEPAS signal is maximized when the tube length is l = 12.4 mm and rapidly decreases when a shorter or longer length is used. This result allows to affirm that the optimal tube length is not dependent from its internal diameter. The internal diameter maximizing the QEPAS signal is ID = 1.59 mm. The 1σ noise level was measured in the same way as reported in Section 4. With the optimal tube geometry (ID = 1.59 mm and l = 12.4 mm), the 1σ noise level results in 0.38 mV, ~1.5 times higher than the value measured for the bare QTF-S08-T. This can be attributed to a small fraction of light hitting the internal surface of tubes. The 1σ noise levels were similar for all spectrophone configurations investigated, within a discrepancy below 5%. The tubes having l = 12.4 mm and ID = 1.59 mm showed the highest SNR of ~1380, as well as the highest QEPAS peak signal (480.8 mV). The QEPAS scan of the water absorption line measured with this spectrophone is shown in Fig. 11(a). The SNR values obtained with the spectrophone system have to be compared with the SNR of the bare QTF. We defined the SNR Enhancement (SNR_E) as the ratio between the SNR measured for the bare QTF and the SNR measured for the QTF coupled with the micro-resonator. In Fig. 11(b), the SNR_E as a function of the internal diameter for tubes having l = 12.4 mm is reported. Starting from the highest value, the SNR_E rapidly decreases when moving to lower inner diameter while the decrease is less pronounced when higher inner diameters are employed.

With QTF-S08-T a signal-to-noise ratio enhancement of ~60 was obtained, which is a new record for mid-IR QEPAS spectroscopy. With respect to the best spectrophone realized with QTF#1, QTF-S08-T reaches a 50% higher SNR_E. This improvement can be ascribed to the T-shape of the prong, although a more detailed calculation is needed to better understand this result.

Optics EXPRESS

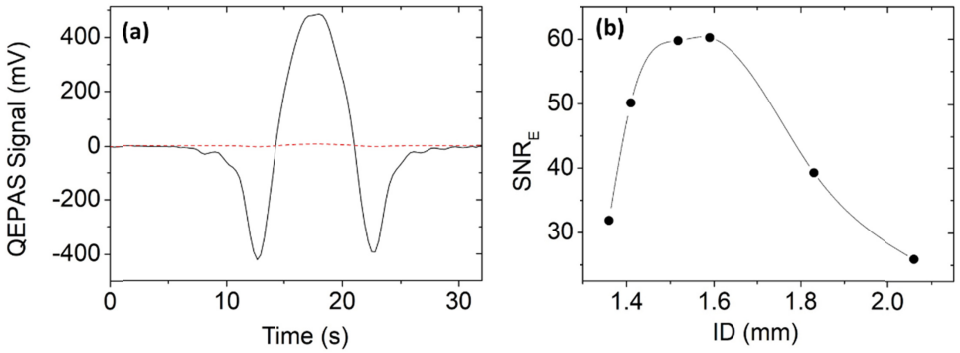

Fig. 11. (a) QEPAS spectral scan of water absorption line acquired with the bare QTF-S08-T (dashed red line) and with a spectrophone composed by QTF-S08-T and a pair of micro-resonator tubes having a length of 12.4 mm and internal diameter of 1.59 mm, both positioned 200 μm far from the QTF (solid black line). (b) Signal-to-noise ratio enhancement (SNR_E) of the spectrophone with respect to the bare QTF as a function of tubes internal diameter when the tube length is 12.4 mm. The solid line is a visual guide.

6. Conclusions

In this work, new designs of quartz tuning forks optimized for QEPAS operation have been investigated. Lowering the resonance frequency while keeping the quality factor high is a straightforward approach to enhance the performance of a QEPAS sensor. Starting from the linear dependence of the quality factor from the prong thickness/length ratio (T/L), combined with the Euler-Bernoulli model for the prediction of the resonance frequency, new designs for QTFs were proposed and realized. The realized QTF possessed a resonance frequency of 15.8 kHz with a quality factor as high as 15,000 at atmospheric pressure. Based on this design, three novel variants were proposed. In the first design, a larger prong spacing was adopted while keeping the same prong geometry, allowing to verify that the resonance properties and Q-factors of a QTF are not affected by prong spacing ≤ 1.5 mm. COMSOL MultiPhysics stress-field simulations were implemented to generate the second design. The simulations demonstrated that the stress field intensity generated by the prong deformation is increased when QTF prongs with a T-shape geometry were employed. With a T-shaped prong geometry, the QTF resonance frequency was reduced to 12.4 kHz while the quality factor was not affected. In the third design, grooves were applied on prongs to increase the coupling between the electrodes, leading to a reduction of the electrical resistance with the quality factor not affected. All novel QTFs were implemented in a QEPAS sensor and tested for the detection of water vapor, exploiting a mid-IR range absorption line. The T-shaped QTF exhibited the best QEPAS performance in terms of the signal-to-noise ratio. Hence, it was selected to be acoustically coupled with a dual-tube micro-resonator system with the aim to enhance the QEPAS sensor performance. Tubes having length of 12.4 mm and an internal diameter of 1.59 mm, positioned about 200 μm far from the QTF surface, provide the best performance in terms of QEPAS SNR optimization. With this condition, an enhancement of the SNR with respect to the bare QTF of a factor of 60 was achieved. The SNR enhancement obtained is a record value for QEPAS systems operating in the mid-IR spectral range. Although the dependence of QEPAS performance on the tube geometry was verified and validated, analytical models proposed in the literature do not allow to exactly predict the acoustic coupling between a QTF a dual-tube system. In order to obtain a more precise estimation of all geometrical parameters involved, it is necessary to develop a theoretical model based on the propagation of the sound wave inside the micro resonator tubes capable to simulate the sound field exiting from tube edges, as a function of the angle with respect to the tube symmetry axis. In this case, the interaction between the exiting sound wave and the QTF

Optics EXPRESS

prongs should be related with the geometrical properties of both acoustic resonators. Hence, the experimental results achieved in this work can be also used as a basis for theoretical and computational approaches (for example, finite element method analysis), mandatory for a precise prediction of an acoustic detection module performance.

Funding

Welch Foundation (Grant C0586).

Acknowledgment

The authors from Dipartimento Interateneo di Fisica di Bari acknowledge financial support from THORLABS GmbH, within the joint-research laboratory PolySense.

References

1. J. Hodgkinson and R. P. Tatam, "Optical gas sensing: a review," Meas. Sci. Technol. **24**(1), 012004 (2013).
2. I. Galli, S. Bartalini, S. Borri, P. Cancio, D. Mazzotti, P. De Natale, and G. Giusfredi, "Molecular gas sensing below parts per trillion: radiocarbon-dioxide optical detection," Phys. Rev. Lett. **107**(27), 270802 (2011).
3. L. Xiong, W. Bai, F. Chen, X. Zhao, F. Yu, and G. J. Diebold, "Photoacoustic trace detection of gases at the parts-per-quadrillion level with a moving optical grating," Proc. Natl. Acad. Sci. U.S.A. **114**(28), 7246–7249 (2017).
4. T. Tomberg, M. Vainio, T. Hieta, and L. Halonen, "Sub-parts-per-trillion level sensitivity in trace gas detection by cantilever-enhanced photo-acoustic spectroscopy," Sci. Rep. **8**(1), 1848 (2018).
5. P. Patimisco, A. Sampaolo, L. Dong, F. K. Tittel, and V. Spagnolo, "Recent advances in quartz enhanced photoacoustic sensing," Appl. Phys. Rev. **5**(1), 011106 (2018).
6. P. Patimisco, G. Scamarcio, F. K. Tittel, and V. Spagnolo, "Quartz-enhanced photoacoustic spectroscopy: a review," Sensors (Basel) **14**(4), 6165–6206 (2014).
7. L. Dong, A. A. Kosterev, D. Thomazy, and F. K. Tittel, "QEPAS spectrophones: design, optimization, and performance," Appl. Phys. B **100**(3), 627–635 (2010).
8. P. Patimisco, A. Sampaolo, H. Zheng, L. Dong, F. K. Tittel, and V. Spagnolo, "Quartz enhanced photoacoustic spectrophones exploiting custom tuning forks: a review," Adv. Phys. X **2**, 169–187 (2016).
9. V. Spagnolo, P. Patimisco, S. Borri, G. Scamarcio, B. E. Bernacki, and J. Kriesel, "Mid-infrared fiber-coupled QCL-QEPAS sensor," Appl. Phys. B **112**(1), 25–33 (2013).
10. G. Wysocki, A. A. Kosterev, and F. K. Tittel, "Influence of molecular relaxation dynamics on quartz-enhanced photoacoustic detection of CO2 at λ =2 μm," Appl. Phys. B **85**(2-3), 301–306 (2006).
11. A. A. Kosterev, T. S. Mosely, and F. K. Tittel, "Impact of humidity on quartz-enhanced photoacoustic spectroscopy based detection of HCN," Appl. Phys. B **85**(2-3), 295–300 (2006).
12. L. Dong, V. Spagnolo, R. Lewicki, and F. K. Tittel, "Ppb-level detection of nitric oxide using an external cavity quantum cascade laser based QEPAS sensor," Opt. Express **19**(24), 24037–24045 (2011).
13. P. Patimisco, S. Borri, A. Sampaolo, H. E. Beere, D. A. Ritchie, M. S. Vitiello, G. Scamarcio, and V. Spagnolo, "A quartz enhanced photo-acoustic gas sensor based on a custom tuning fork and a terahertz quantum cascade laser," Analyst (Lond.) **139**(9), 2079–2087 (2014).
14. A. Sampaolo, P. Patimisco, M. Giglio, M. S. Vitiello, H. E. Beere, D. A. Ritchie, G. Scamarcio, F. K. Tittel, and V. Spagnolo, "Improved tuning fork for terahertz quartz-enhanced photoacoustic spectroscopy," Sensors (Basel) **16**(4), 439–446 (2016).
15. H. Zheng, L. Dong, A. Sampaolo, P. Patimisco, W. Ma, L. Zhang, W. Yin, L. Xiao, V. Spagnolo, S. Jia, and F. K. Tittel, "Overtone resonance enhanced single-tube on-beam quartz enhanced photoacoustic spectrophone," Appl. Phys. Lett. **109**(11), 111103 (2016).
16. A. Sampaolo, P. Patimisco, L. Dong, A. Geras, G. Scamarcio, T. Starecki, F. K. Tittel, and V. Spagnolo, "Quartz-enhanced photoacoustic spectroscopy exploiting tuning fork overtone modes," Appl. Phys. Lett. **107**(23), 231102 (2015).
17. F. K. Tittel, A. Sampaolo, P. Patimisco, L. Dong, A. Geras, T. Starecki, and V. Spagnolo, "Analysis of overtone flexural modes operation in quartz-enhanced photoacoustic spectroscopy," Opt. Express **24**(6), A682–A692 (2016).
18. H. Zheng, L. Dong, P. Patimisco, H. Wu, A. Sampaolo, X. Yin, S. Li, W. Ma, L. Zhang, W. Yin, L. Xiao, V. Spagnolo, S. Jia, and F. K. Tittel, "Double antinode excited quartz-enhanced photoacoustic spectrophone," Appl. Phys. Lett. **110**(2), 021110 (2017).
19. H. Wu, X. Yin, L. Dong, K. Pei, A. Sampaolo, P. Patimisco, H. Zheng, W. Ma, L. Zhang, W. Yin, L. Xiao, V. Spagnolo, S. Jia, and F. K. Tittel, "Simultaneous dual-gas QEPAS detection based on a fundamental and overtone combined vibration of quartz tuning fork," Appl. Phys. Lett. **110**(12), 121104 (2017).
20. P. Patimisco, A. Sampaolo, L. Dong, M. Giglio, G. Scamarcio, F. K. Tittel, and V. Spagnolo, ""Analysis of the electro-elastic properties of custom quartz tuning forks for optoacoustic gas sensing," Sensor Actuat," Biol. Chem. **227**, 539–546 (2016).

Optics EXPRESS

21. P. Patimisco, A. Sampaolo, V. Mackowiak, H. Rossmadl, A. Cable, F. K. Tittel, and V. Spagnolo, "Loss mechanisms determining the quality factors in quartz tuning forks vibrating at the fundamental and first overtone mode," IEEE T. Ultrason. Ferr. *10.1109/TUFFC.2018.2853404*.
22. F. R. Blom, S. Bouwstra, M. Elwenspoek, and J. H. J. Fluitman, "Dependence of the quality factor of micromachined silicon beam resonators on pressure and geometry," J. Vac. Sci. Technol. B **10**(1), 19–26 (1992).
23. Y. Jimbo and K. Itao, "Energy loss of a cantilever vibrator," J. Horological Inst. Jpn. **47**, 1–15 (1968).
24. C. Zener, "Internal friction in solids II. General theory of thermoelastic internal friction," Phys. Rev. **53**(1), 90–99 (1930).
25. P. Patimisco, A. Sampaolo, M. Giglio, V. Mackowiak, H. Rossmadl, B. Gross, A. Cable, F. K. Tittel, and V. Spagnolo, "Octupole electrode pattern for tuning forks vibrating at the first overtone mode in quartz-enhanced photoacoustic spectroscopy," Opt. Lett. **43**(8), 1854–1857 (2018).
26. A. Castellanos-Gomez, N. Agraït, and G. Rubio-Bollinger, "Dynamics of quartz tuning fork force sensors used in scanning probe microscopy," Nanotechnology **20**(21), 215502 (2009).
27. M. Hirata, K. Kokubun, M. Ono, and K. Nakayama, "Size effect of a quartz oscillator on its characteristics as a friction vacuum gauge," J. Vac. Sci. Technol. A **3**(3), 1742–1745 (1985).
28. Y. Qin and R. Reifenberger, "Calibrating a tuning fork for use as a scanning probe microscope force sensor," Rev. Sci. Instrum. **78**(6), 063704 (2007).
29. H. Hosaka, K. Itao, and S. Kuroda, "Damping characteristics of beam-shaped micro-oscillators," Sensor. Actuat. A-Phys. **49**, 87–95 (1995).
30. Z. Hao, A. Erbil, and F. Ayazi, "An analytical model for support loss in micromachined beam resonators with in-plane flexural vibrations," Sensor. Actuat," A-Phys. **109**, 156–164 (2003).
31. http://www.hitran.org/